An Integrator Backstepping-Based Algorithm for Spacecraft's Effective Surface Tracking

Alessio Bocci[1st], Juan Corona-Sanchez[2nd], Raymond Kristiansen[3rd]
Faculty of Electrical Engineering, Science and Technology
UiT – The Arctic University of Norway
Narvik, Norway
alessio.bocci@uit.no, jose.j.sanchez@uit.no, and raymond.kristiansen@uit.no

***Abstract*—CubeSats are widely used in space missions due to their low cost and versatility, but their lack of propulsion severely limits orbital control. As a result, passive control strategies are commonly adopted, with drag-based control being the most prominent. This approach exploits attitude maneuvers to modulate the spacecraft's effective surface, defined as the cross-sectional area exposed to the atmosphere–spacecraft relative velocity. This paper proposes a novel attitude-control framework for tracking a desired effective-surface profile. First, the effective surface and its dynamics are formally defined. Then, an attitude control law based on the integrator backstepping technique is developed to achieve effective-surface tracking. Finally, simulation results show the effectiveness of the proposed method.**

***Index Terms*—Attitude control, surface control, aerodynamic control, optimization**

I. INTRODUCTION

Passively controlling a single satellite or a group of satellites via aerodynamic forces is a well-established research area spanning several closely related yet distinct topics. In Low Earth Orbit (LEO), atmospheric interaction can be exploited to control a spacecraft's orbit with inherently low control authority. This makes the approach suitable for missions with coarse accuracy requirements and, as an auxiliary method, for large spacecraft needing minor corrections. The current shift from single spacecraft to distributed CubeSats further increases the relevance of aerodynamic-based techniques—especially differential drag—as a primary means of control.

When multiple satellites are involved, distinction must be made between constellations and formation flying. Formation flying typically involves intersatellite communication to perform cooperative maneuvers, whereas constellations may not require as tight coordination. Although many aerodynamic-control techniques are applicable to both settings, they generally require mission-dependent adaptation.

Aerodynamic forces are lift and drag. Lift is usually small and is mainly useful for minor out-of-plane adjustments [1], [2]; accordingly, it is often neglected (as in this study). Drag-based control—particularly differential drag—is widely used for station-keeping [3], docking, constellation establishment and maintenance [4]–[7], and formation-flying management.

Drag-based control is formulated in terms of variations in the ballistic coefficient (mass divided by drag coefficient times cross-sectional area). For a propulsionless CubeSat, mass is effectively constant; moreover, the drag coefficient is typically constant for a given vehicle and often similar across multiple spacecraft with comparable geometries. Thus, the practical control lever is the modulation of the exposed area.

This paper introduces the concept of the spacecraft's effective surface (ES), *i.e.*, the surface that can generate a net drag force per unit mass to alter orbital motion. Depending on the platform, this can be achieved through dedicated hardware (*e.g.*, tiltable drag panels) or, more commonly for CubeSats, through attitude maneuvers.

Although aerodynamic orbit control is a coupled six-degrees-of-freedom problem [8]–[12], attitude dynamics primarily act as the mechanism to vary the ES. Hence, as a first approximation, it is reasonable to separate orbital dynamics design (translational motion) from attitude dynamics (rotational motion): first, synthesize a desired ES profile that yields the required orbital behavior, then derive the rotations and control torques needed to realize that profile.

Early differential-drag formation-keeping was pioneered by Leonard et al. [13]. Under the assumptions of uniform atmospheric density and initially equal velocities and ballistic coefficients, they proposed an on–off strategy that varies the drag-panel angle of attack between $0 - 90$ deg to generate differential drag. Their two-part control law drives the relative position to a target value and minimizes the eccentricity of the relative-motion ellipse in the Hill frame.

Kumar et al. [14] further assessed the feasibility of nano-satellite formation control by identifying suitable altitude ranges and proposing a surface-modulation strategy based on orbital energy comparisons. For a two-spacecraft formation, they designed a proportional-integral-derivative controller that commands ES changes to either the leader or the follower based on the sign of the orbital energy difference.

Shouman and Atallah [15] designed a linear quadratic regulator (LQR) for relative positioning based on modified Hill's equations that account for both drag and Earth's oblateness.

The above works primarily determine the required ES from an orbital-control perspective, without explicitly addressing how the vehicle should realize that surface. For small satellites where attitude maneuvers are preferred over tiltable panels, Ivanov et al. [2] modeled differential drag for two identical

Work funded by the Research Council of Norway. Project 335832.

spherical spacecraft with thin solar panels. They expressed the differential-drag force in terms of physical parameters and two unit vectors (the panel normal and the incoming flow direction), and then reparameterized it as a function of four attitude angles (two latitudes and two longitudes). Their approach uses LQR for orbital control and then solves nonlinear equations at each time instant to recover the attitude angles. A key limitation is that the nonlinear system may admit no solution, a unique solution, or two solutions depending on the LQR command magnitude, and the solution can be computationally demanding.

An alternative coupled orbital-attitude approach is proposed by Harris et al. [6], [16], [17], using modified Rodrigues parameters. They derive a linear system that couples relative orbital dynamics with attitude dynamics and then design an LQR controller for the combined model.

Against this background, this paper proposes a new solution to the ES tracking problem. It first defines ES dynamics as a function of spacecraft angular velocity and the orbital state vector, then applies integrator backstepping to compute the angular-velocity command needed to track a desired ES profile and the corresponding control torque.

The core idea is to enforce an angular-velocity that yields the desired ES while allowing the attitude to evolve accordingly, in contrast to standard attitude control, which drives both angular velocity and attitude to prescribed references.

II. PRELIMINARIES

This section introduces the reference frames, the scientific notation, and the fundamental equations used in the work.

Referring to Fig. 1, we use two reference frames: the Earth-Centered Inertial frame (ECI), denoted by $\mathcal{F}_i$ (quantities with superscript i), and the spacecraft body frame, denoted by $\mathcal{F}_b$ (quantities with superscript b).

$\mathcal{F}_i$ is a nonrotating right-handed inertial frame, with the x^i-axis aligned with the vernal equinox, the x^i–y^i plane coincident with the Earth's equatorial plane, and the z^i-axis pointing northward along the Earth's rotation axis [18].

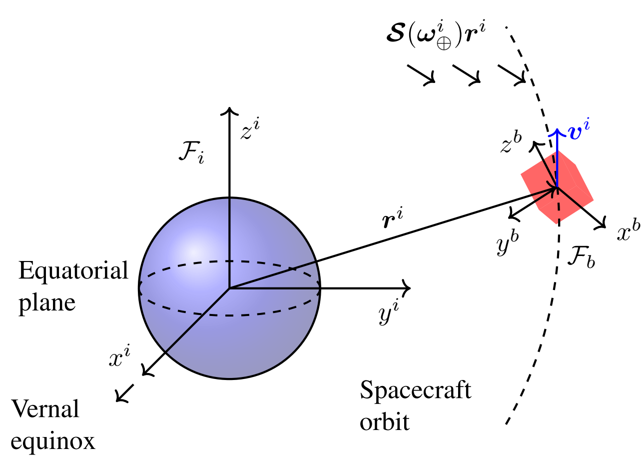

Fig. 1. Reference frames.

$\mathcal{F}_b$ is a right-handed body-fixed frame centered at the spacecraft center of mass and aligned with the principal inertia axes. Its orientation with respect to $\mathcal{F}_i$ is described by the rotation matrix $\mathbf{R}_i^b \in \mathrm{SO}(3)$, such that $\boldsymbol{x}^b = \mathbf{R}_i^b \boldsymbol{x}^i$.

For $\{\boldsymbol{x}, \boldsymbol{y}\} \in \mathbb{R}^3$, the cross product can be expressed as

$$\boldsymbol{x} \times \boldsymbol{y} = \boldsymbol{\mathcal{S}}(\boldsymbol{x})\boldsymbol{y}, \quad \boldsymbol{\mathcal{S}}(\boldsymbol{x}) = \begin{bmatrix} 0 & -x_3 & x_2 \\ x_3 & 0 & -x_1 \\ -x_2 & x_1 & 0 \end{bmatrix}.$$

For a LEO orbiting spacecraft, the drag acceleration is $\boldsymbol{a}_D^i = -\beta S \|\boldsymbol{w}^i\| \boldsymbol{w}^i$, where $\boldsymbol{w}^i = \boldsymbol{v}^i - \boldsymbol{\mathcal{S}}(\boldsymbol{\omega}_\oplus^i)\boldsymbol{r}^i$, $\beta = \rho C_D/(2M)$, $\boldsymbol{r}^i$ and $\boldsymbol{v}^i$ are the spacecraft's position and velocity vector, S is the ES, C_D is the drag coefficient ($\approx$ 2.2 [19]), M is the mass, $\rho(h)$ is the atmosphere density, $h = \|\boldsymbol{r}^i\| - R_\oplus$ is the altitude, $R_\oplus = 6371$ km is the Earth's radius, and $\boldsymbol{\omega}_\oplus^i = [0, 0, 7.292115486 \times 10^{-5}]^\top$ rad/s is the Earth's angular velocity. Thus, the two-body problem is [18]

$$\ddot{\boldsymbol{r}}^i = -\frac{\mu}{\|\boldsymbol{r}^i\|^3}\boldsymbol{r}^i - \beta S \|\boldsymbol{w}^i\| \boldsymbol{w}^i \tag{1}$$

where $\mu = 398600\ \mathrm{km^3/s^2}$ is the Earth's gravitational constant. Let $\mathbf{I}_3 \in \mathbb{R}^{3\times 3}$ be the identity matrix, we define $\boldsymbol{\xi}$ and $\dot{\boldsymbol{\xi}}$ as

$$\boldsymbol{\xi} = \frac{\boldsymbol{w}^i}{\|\boldsymbol{w}^i\|}, \quad \dot{\boldsymbol{\xi}} = \frac{\boldsymbol{\xi}\boldsymbol{\xi}^\top - \mathbf{I}_3}{\|\boldsymbol{w}^i\|}\left[\boldsymbol{\mathcal{S}}(\boldsymbol{\omega}_\oplus^i)\boldsymbol{v}^i + \frac{\mu}{\|\boldsymbol{r}^i\|^3}\boldsymbol{r}^i\right]. \tag{2}$$

Finally, the attitude kinematics and the Euler equations are

$$\dot{\mathbf{R}}_i^b = -\boldsymbol{\mathcal{S}}(\boldsymbol{\omega}^b)\mathbf{R}_i^b \tag{3}$$
$$\mathbf{J}\dot{\boldsymbol{\omega}}^b = \boldsymbol{\mathcal{S}}(\mathbf{J}\boldsymbol{\omega}^b)\boldsymbol{\omega}^b + \boldsymbol{u}^b \tag{4}$$

where $\boldsymbol{\omega}$ is the spacecraft's angular velocity, $\mathbf{J}$ is the symmetric and positive definite (SPD) inertia tensor, and $\boldsymbol{u}$ is the control input. For notational simplicity, the superscript b is omitted hereafter, as all these quantities are expressed in $\mathcal{F}_b$.

III. EFFECTIVE SURFACE AND ITS DYNAMICS

The ES is the spacecraft cross-sectional area projected along $\boldsymbol{\xi}$ and directly relates to the drag force. Detailed derivations based on molecular–surface interaction models are provided in [20], while for complex spacecraft geometries, the ES can be evaluated using advanced methods [21]. In this paper, we adopt the model presented in [19], where the ES is defined as

$$S = \sum_{j=1}^{n} \boldsymbol{\eta}^\top \boldsymbol{n}_j^b S_j, \quad \boldsymbol{\eta} = \mathbf{R}\boldsymbol{\xi} \tag{5}$$

where n is the number of surfaces, and $\boldsymbol{n}_j^b$ is the unit vector normal to the j-th surface S_j. The standard CubeSat setup is summarized in Table I. Because only positive terms in (5) must be summed up, we rearrange the equation as

$$S = \frac{1}{2}\sum_{j=1}^{6} \phi_j S_j, \quad \phi_j = \boldsymbol{\eta}^\top \boldsymbol{n}_j^b \left[1 + \mathrm{sgn}\left(\boldsymbol{\eta}^\top \boldsymbol{n}_j^b\right)\right] \tag{6}$$

By splitting the summation in (6) and using Table I, we get

$$\mathfrak{S}_1 = \frac{1}{2}\sum_{j=1}^{3}\phi_j S_j = \frac{1}{2}\left[\boldsymbol{s}^\top\boldsymbol{\eta} + \boldsymbol{m}^\top\boldsymbol{\sigma}\boldsymbol{\eta}\right]$$
$$\mathfrak{S}_2 = \frac{1}{2}\sum_{j=4}^{6}\phi_j S_j = \frac{1}{2}\left[-\boldsymbol{s}^\top\boldsymbol{\eta} + \boldsymbol{m}^\top\boldsymbol{\sigma}\boldsymbol{\eta}\right]$$

with $\boldsymbol{s} = [S_1, S_2, S_3]^\top$, $\boldsymbol{\sigma} = \mathrm{diag}(\boldsymbol{s})$, and $\boldsymbol{m} = \mathrm{sgn}(\boldsymbol{\eta})$, where we used the operator signum of a vector defined as $\mathrm{sgn}(\boldsymbol{\eta}) = [\mathrm{sgn}(\eta_1), \mathrm{sgn}(\eta_2), \mathrm{sgn}(\eta_3)]^\top$. Hence, using (3), the ES and its dynamics become

$$S = \mathfrak{S}_1 + \mathfrak{S}_2 = \boldsymbol{m}^\top\boldsymbol{\sigma}\boldsymbol{\eta} \tag{7}$$
$$\dot{S} = \dot{\boldsymbol{m}}^\top\boldsymbol{\sigma}\boldsymbol{\eta} + \boldsymbol{m}^\top\boldsymbol{\sigma}\boldsymbol{\mathcal{S}}(\boldsymbol{\eta})\boldsymbol{\omega} + \boldsymbol{m}^\top\boldsymbol{\sigma}\mathbf{R}\dot{\boldsymbol{\xi}}. \tag{8}$$

TABLE I
CUBESATS SURFACES AND NORMALS.

Surface	Value	Unit Vector
1	S_1	$\boldsymbol{n}_1^b = [1, 0, 0]^\top$
2	S_2	$\boldsymbol{n}_2^b = [0, 1, 0]^\top$
3	S_3	$\boldsymbol{n}_3^b = [0, 0, 1]^\top$
4	$S_4 = S_1$	$\boldsymbol{n}_4^b = -\boldsymbol{n}_1^b$
5	$S_5 = S_2$	$\boldsymbol{n}_5^b = -\boldsymbol{n}_2^b$
6	$S_6 = S_3$	$\boldsymbol{n}_6^b = -\boldsymbol{n}_3^b$

Note that (7) defines S as a continuous but non-differentiable function at $\eta_j = 0$, implying that $\dot{S}$ involves $\dot{\boldsymbol{m}}$, *i.e.*, Dirac delta terms. This issue is addressed in the next section. To the authors' knowledge, such a general ES matrix formulation has not been previously reported in the literature.

IV. SPACECRAFT CONFIGURATIONS

The main issue with (8) is the non-differentiability in $\eta_j = 0$. This fact makes Lyapunov theory, strictly speaking, inapplicable. This problem may be solved in two ways. The first is to assume that the spacecraft always remains in one of the configurations of Table II during the control operations, where $\boldsymbol{m}$ is fixed and S is a class $\mathcal{C}^2$ function. The second is to treat the problem as a hybrid system and prove asymptotic stability accordingly [22], [23].

In this work, we choose the first option and, thus, we state the following configuration-belonging requirement:

Requirement 1. *If the spacecraft at $t = \hat{t} \geq 0$ is in a configuration defined by $\hat{\boldsymbol{m}} = \mathrm{sgn}(\boldsymbol{\eta})|_{t=\hat{t}}$, then, $\forall t \geq \hat{t}$, the rotation profile $\mathbf{R}$ must be such that $\boldsymbol{m} = \hat{\boldsymbol{m}}\,\forall t \geq \hat{t}$, i.e.*

$$\mathrm{diag}(\hat{\boldsymbol{m}})\boldsymbol{\eta} = \mathrm{diag}(\hat{\boldsymbol{m}})\mathbf{R}\boldsymbol{\xi} \geq 0 \quad \forall t \geq \hat{t} \geq 0\,. \tag{9}$$

This requirement mandates that the spacecraft uses only the three surfaces "active" at $t = \hat{t}$. Although this requirement restricts maneuverability, it is practically feasible and enables the design of configuration-based Lyapunov controllers.

Table II shows that there are eight possible configurations. Let $\boldsymbol{s}_m = \boldsymbol{\sigma}\hat{\boldsymbol{m}}$, then (7) and (8) can be rewritten as

$$S = \boldsymbol{s}_m^\top\boldsymbol{\eta}, \quad \dot{S} = \boldsymbol{s}_m^\top\boldsymbol{\mathcal{S}}(\boldsymbol{\eta})\boldsymbol{\omega} + \boldsymbol{s}_m^\top\mathbf{R}\dot{\boldsymbol{\xi}}\,. \tag{10}$$

TABLE II
POSSIBLE SURFACES CONFIGURATIONS.

Config.	Surfaces	$\boldsymbol{m} = \mathrm{sgn}(\boldsymbol{\eta})$
I	1, 2, 3	$\boldsymbol{m} = [1, 1, 1]^\top$
II	1, 2, 6	$\boldsymbol{m} = [1, 1, -1]^\top$
III	1, 5, 3	$\boldsymbol{m} = [1, -1, 1]^\top$
IV	1, 5, 6	$\boldsymbol{m} = [1, -1, -1]^\top$
V	4, 2, 3	$\boldsymbol{m} = [-1, 1, 1]^\top$
VI	4, 2, 6	$\boldsymbol{m} = [-1, 1, -1]^\top$
VII	4, 5, 3	$\boldsymbol{m} = [-1, -1, 1]^\top$
VIII	4, 5, 6	$\boldsymbol{m} = [-1, -1, -1]^\top$

The goal is to track a desired rotation profile $\boldsymbol{\omega}_d$ that ensures the spacecraft satisfies (9). In this work, $\boldsymbol{\omega}_d$ is not determined a priori, but it is an output of the integrator backstepper.

V. INTEGRATOR BACKSTEPPING CONTROL

This section presents a proposition for the attitude-based ES tracking. Let S_d be the desired ES profile and assume that $S_d(t)$ and $\dot{S}_d(t)$ are bounded functions. We define the ES error and its dynamics as

$$S_e = S - S_d, \quad \dot{S}_e = f + \boldsymbol{g}^\top\boldsymbol{\omega} \tag{11}$$

with $f = \boldsymbol{s}_m^\top\mathbf{R}\dot{\boldsymbol{\xi}} - \dot{S}_d$ and $\boldsymbol{g} = -\boldsymbol{\mathcal{S}}(\boldsymbol{\eta})\boldsymbol{s}_m$. From this, we now state our main result:

Proposition 1. *Assume $\boldsymbol{m} = \hat{\boldsymbol{m}}\ \forall t \geq \hat{t}$ as per Req. 1. Moreover, let $\boldsymbol{\omega}_e = \boldsymbol{\omega} - \boldsymbol{\omega}_d$ and $\boldsymbol{\omega}_d$ be the solution of the consistent-underdetermined linear system*

$$f + \boldsymbol{g}^\top\boldsymbol{\omega}_d = -k_s S_e\,. \tag{12}$$

Then, the equilibrium point $(S_e, \boldsymbol{\omega}_e) = (0, \mathbf{0})$ of the error dynamics $\{\dot{S}_e, \dot{\boldsymbol{\omega}}_e\}$ is asymptotically stable, if the dynamics (4) *is in closed-loop with the control law*

$$\boldsymbol{u} = -\boldsymbol{\mathcal{S}}(\mathbf{J}\boldsymbol{\omega})\boldsymbol{\omega} + \mathbf{J}\dot{\boldsymbol{\omega}}_d - \boldsymbol{g}S_e - \mathbf{K}_\omega\boldsymbol{\omega}_e \tag{13}$$

with $\mathbf{K}_\omega \in \mathbb{R}^{3\times3}$ SPD and $k_s > 0$ feedback gains.

Proof. The proof follows classical steps of the integrator backstepping technique –*cf.* Khalil [24]. Let $V\colon \mathbb{R} \to \mathbb{R}$ be a continuously differentiable Lyapunov function such that $V(0) = 0$ and $V(S_e) > 0$ in $\mathbb{R} - \{0\}$ defined as $V = S_e^2/2$.

By taking the time derivative, we get $\dot{V} = S_e(f + \boldsymbol{g}^\top\boldsymbol{\omega})$. Thus, by choosing $\boldsymbol{\omega} \equiv \boldsymbol{\omega}_d$ such that $f + \boldsymbol{g}^\top\boldsymbol{\omega}_d = -k_s S_e$ with $k_s > 0$, we end up with $\dot{V} = -k_s S_e^2$. Since $V(0) = 0$, $V(S_e) > 0 \forall S_e \neq 0$, and $\dot{V}(S_e) < 0 \forall S_e \neq 0$, the origin $S_e = 0$ of (11) is asymptotically stable.

To perform the backstepping, we define $\boldsymbol{\omega}_e = \boldsymbol{\omega} - \boldsymbol{\omega}_d$. By taking the time derivative and using (4), we get

$$\mathbf{J}\dot{\boldsymbol{\omega}}_e = \boldsymbol{\mathcal{S}}(\mathbf{J}\boldsymbol{\omega})\boldsymbol{\omega} - \mathbf{J}\dot{\boldsymbol{\omega}}_d + \boldsymbol{u}. \tag{14}$$

Finally, let $V_c\colon \mathbb{R}\times\mathbb{R}^3 \to \mathbb{R}$ be a continuously differentiable composite Lyapunov function such that $V_c(0, \mathbf{0}) = 0$ and $V_c(S_e, \boldsymbol{\omega}_e) > 0$ in $\mathbb{R} \times \mathbb{R}^3 - \{0, \mathbf{0}\}$ defined as $V_c =$

$S_e^2/2 + \boldsymbol{\omega}_e^\top \mathbf{J}\boldsymbol{\omega}_e/2$. By taking its time derivative, we get $\dot{V}_c = -k_s S_e^2 + \boldsymbol{\omega}_e^\top [\boldsymbol{g}S_e + \boldsymbol{\mathcal{S}}(\mathbf{J}\boldsymbol{\omega})\boldsymbol{\omega} - \mathbf{J}\dot{\boldsymbol{\omega}}_d + \boldsymbol{u}]$.

By defining $\boldsymbol{u} = -\boldsymbol{\mathcal{S}}(\mathbf{J}\boldsymbol{\omega})\boldsymbol{\omega} + \mathbf{J}\dot{\boldsymbol{\omega}}_d - \boldsymbol{g}S_e - \mathbf{K}_\omega\boldsymbol{\omega}_e$ with $\mathbf{K}_\omega$ SPD, we end up with $\dot{V}_c = -k_s S_e^2 - \boldsymbol{\omega}_e^\top \mathbf{K}_\omega \boldsymbol{\omega}_e$.

Hence, since $V_c(0,\mathbf{0}) = 0$, $V_c(S_e,\boldsymbol{\omega}_e) > 0\,\forall(S_e,\boldsymbol{\omega}_e) \neq (0,\mathbf{0})$, and $\dot{V}_c(S_e,\boldsymbol{\omega}_e) < 0\,\forall(S_e,\boldsymbol{\omega}_e) \neq (0,\mathbf{0})$, the equilibrium point $(S_e,\boldsymbol{\omega}_e) = (0,\mathbf{0})$ of the system (11) and (14) is asymptotically stable [24]. □

VI. Constrained Minimization Problem

The main issue of Prop. 1 is solving (12) to get $\boldsymbol{\omega}_d$. Since the latter is one equation with three unknowns, it admits infinitely many solutions forming a two-dimensional solution space, according to the Rouché–Capelli theorem [25]. In addition, the solution $\boldsymbol{\omega}_d$ must satisfy Req. 1.

Our solution strategy is a constrained minimization. Given the nature of the constraints (9), the solution is obtained via quadratic programming (QP), with constraints expressed using control barrier functions (CBFs). The required background is briefly reviewed before applying the methodology.

Following Ames et al. [26], the safe set $\mathcal{C}$ is defined as the superlevel set of a continuously differentiable function $h\colon D \subset \mathbb{R}^n \to \mathbb{R}$ such that

$$\begin{aligned} \mathcal{C} &= \{x \in D \subset \mathbb{R}^n \colon h(x) \geq 0\} \\ \partial\mathcal{C} &= \{x \in D \subset \mathbb{R}^n \colon h(x) = 0\} \\ \mathrm{Int}(\mathcal{C}) &= \{x \in D \subset \mathbb{R}^n \colon h(x) > 0\}\,. \end{aligned}$$

We now introduce the following definitions and theorem:

Definition 1. *Let $\boldsymbol{x} \in \mathbb{R}^n$ and $\boldsymbol{f}\colon \mathbb{R}^n \to \mathbb{R}^n$. Then, the set $\mathcal{C}$ is said to be forward invariant for system $\dot{\boldsymbol{x}} = \boldsymbol{f}(\boldsymbol{x})$ if $\forall \boldsymbol{x}_0 \in \mathcal{C}$, $\boldsymbol{x}(t) \in \mathcal{C}$ for $\boldsymbol{x}(t_0) = \boldsymbol{x}_0$ and $\forall t \geq t_0 \geq 0$.*

Definition 2. *Let $j = 1,\ldots,m$, $\boldsymbol{x} \in \mathbb{R}^n$, $\boldsymbol{f}\colon \mathbb{R}^n \to \mathbb{R}^n$, and $h\colon D \subset \mathbb{R}^n \times \mathbb{R}_{\geq 0} \to \mathbb{R}$ a continuously differentiable function. Moreover, let $\psi_0(\boldsymbol{x},t) = h(\boldsymbol{x},t)$, $\psi_j\colon D \subset \mathbb{R}^n \times \mathbb{R}_{\geq 0} \to \mathbb{R}$ defined as $\psi_j(\boldsymbol{x},t) = \dot{\psi}_{j-1}(\boldsymbol{x},t) + \alpha_j(\psi_{j-1}(\boldsymbol{x},t))$, and $\mathcal{C}_j \subset D \subset \mathbb{R}^n$ defined as $\mathcal{C}_j = \{\boldsymbol{x} \in \mathbb{R}^n \colon \psi_{j-1}(\boldsymbol{x},t) \geq 0\}$. Then, the function h is said to be a High-Order Control Barrier Function (HOCBF) of relative degree m for the dynamics $\dot{\boldsymbol{x}} = \boldsymbol{f}(\boldsymbol{x})$ if there exist differentiable class $\mathcal{K}$ functions α_j such that*

$$\psi_m(\boldsymbol{x},t) \geq 0\,\forall(\boldsymbol{x},t) \in \mathcal{C}_1\cap,\ldots,\cap\mathcal{C}_m \times \mathbb{R}_{\geq 0}\,.$$

Theorem 1. *Let $\boldsymbol{x} \in \mathbb{R}^n$, $\boldsymbol{f}\colon \mathbb{R}^n \to \mathbb{R}^n$, and $h\colon D \subset \mathbb{R}^n \times \mathbb{R}_{\geq 0} \to \mathbb{R}$ a continuously differentiable function. Then, the set $\mathcal{C}_1\cap,\ldots,\cap\mathcal{C}_m \times \mathbb{R}_{\geq 0}$ is forward invariant for system $\dot{\boldsymbol{x}} = \boldsymbol{f}(\boldsymbol{x})$ if $h(\boldsymbol{x},t)$ is an HOCBF.*

In our notation, $\mathbb{R}_{\geq 0}$ is the set of positive real numbers. Def. 1, Def. 2 and Theorem 1, taken from [27], provide forward invariance conditions based on HOCBFs, applicable when the constraint has relative degree greater than one. In the CBF case, the iteration stops at $m = 1$. For (9), we get

$$\begin{aligned} \boldsymbol{h}(\boldsymbol{\eta}) &= \mathrm{diag}(\hat{\boldsymbol{m}})\boldsymbol{\eta} - \boldsymbol{\epsilon} \Rightarrow \boldsymbol{\psi}_0(\boldsymbol{\eta}) = \boldsymbol{h}(\boldsymbol{\eta}) \\ \boldsymbol{\psi}_1(\boldsymbol{\eta}) &= \dot{\boldsymbol{\psi}}_0(\boldsymbol{\eta}) + \boldsymbol{\alpha}_1(\boldsymbol{\psi}_0(\boldsymbol{\eta})) \end{aligned}$$

where $\boldsymbol{\epsilon} > \mathbf{0}$ is a safety margin. Hence, for Def. 2, it must be

$$\mathrm{diag}(\hat{\boldsymbol{m}})\boldsymbol{\mathcal{S}}(\boldsymbol{\eta})\boldsymbol{\omega}^b + \mathrm{diag}(\hat{\boldsymbol{m}})\mathbf{R}\dot{\boldsymbol{\xi}} + \boldsymbol{\alpha}_1(\boldsymbol{h}(\boldsymbol{\eta})) \geq \mathbf{0}\,.$$

Thus, the minimization problem formalizes into

$$\begin{aligned} \min_{(\boldsymbol{\omega}_d,\delta)\in\mathbb{R}^4} \quad & \frac{1}{2}\boldsymbol{\omega}_d^\top \mathbf{H}\boldsymbol{\omega}_d + \frac{p}{2}\delta^2 \\ \text{subjected to} \quad & \mathbf{A}_{eq}\boldsymbol{\omega}_d = b_{eq} + \delta \\ & \mathbf{A}_{cbf}\boldsymbol{\omega}_d \geq \boldsymbol{b}_{cbf} \end{aligned} \tag{15}$$

with $\mathbf{A}_{eq} = \boldsymbol{g}^\top$, $b_{eq} = -k_s S_e - f$, $\mathbf{A}_{cbf} = \mathrm{diag}(\hat{\boldsymbol{m}})\boldsymbol{\mathcal{S}}(\boldsymbol{\eta})$, and $\boldsymbol{b}_{cbf} = -\mathrm{diag}(\hat{\boldsymbol{m}})\mathbf{R}\dot{\boldsymbol{\xi}} - \boldsymbol{\alpha}_1(\boldsymbol{h}(\boldsymbol{\eta}))$. Moreover, $\mathbf{H}$ is any SPD matrix, and δ is a slack variable weighted by $p > 0$ to ensure QP feasibility. Introducing slack variables on the equality constraints allows temporary relaxation of stabilization objectives, while the safety constraints remain strictly enforced.

VII. Simulation and Results

This section assesses the tracking accuracy of the control law derived in Section V through a simulated case. The simulation parameters and initial conditions are reported in Table III and Table IV, respectively.

The spacecraft is initially orbiting on a 450 km-altitude quasi-circular polar orbit of period $T = 1.5831\,\mathrm{h}$. Control is initiated after detumbling $\boldsymbol{\omega}(0) = \mathbf{0}$ rad/s and in configuration I of Table II.

According to the literature [28], two ES profiles are commonly adopted. A periodic profile, $S_d(t) = \hat{S}\sin(\nu t + \varphi) + \bar{S}$, generates bounded relative motion, yielding closed elliptical trajectories in the Hill frame. An exponentially damped profile, $S_d(t) = \hat{S}\exp(-\zeta\nu t)\sin(\nu_d t + \varphi) + \bar{S}$, is instead used to drive the intersatellite distance toward a fixed equilibrium. The latter was used in the simulation because it allows us to study both the oscillatory and steady-state profiles simultaneously.

Simulations were performed over $2T$ with a sampling time of 0.1 s, using Simulink and a 4th-order Runge-Kutta integration scheme. The minimization problem (15) was solved using the *quadprog* solver with the *interior-point-convex* algorithm.

The function $\boldsymbol{\alpha}_1$ was assumed to be $\boldsymbol{\alpha}_1(\boldsymbol{\psi}_0) = \gamma\boldsymbol{\psi}_0$ with $\gamma \geq 0$, and the penalty p was chosen high to make the equality constraint hard and test the numerical robustness.

Fig. 2 shows two attempts of transition at the locations indicated by the dashed lines, first from configuration I to II at approximately $0.11T$ and later from configuration I to III at about $0.6T$, occurring when the S_d oscillation amplitudes are the highest. In these instances, the CBF constraints become active, modifying the angular velocity to enforce safety. As the oscillation amplitude subsequently decreases, the QP yields a $\boldsymbol{\omega}_d$ profile that no longer drives the system toward the configuration boundaries. This behavior is also inherent to the CBF formulation, which intrinsically reshapes the admissible set near the configuration boundary.

It is worth noting that the angular velocity $\boldsymbol{\omega}$ does not converge to zero. As shown by (10), an additional perturbative term—negligible during the transient—must be compensated at steady state. This term is related to $\dot{\boldsymbol{\xi}}$ and reflects the fact that, in general, a constant ES is not a natural equilibrium and must be actively enforced (except for spherical spacecraft).

Finally, Fig. 3 shows that the composite Lyapunov function and the ES error decrease monotonically, in agreement with the theoretical results established in Section V.

TABLE III
SIMULATION PARAMETERS

Qty.	Value	Units
$\boldsymbol{s}$	$[S_1, S_2, S_3]^\top = [350, 500, 800]^\top$	cm^2
$\hat{S}$	300	cm^2
$\bar{S}$	700	cm^2
T	1.5831	h
φ	-10.3948	rad
ν	0.0024245	rad/s
ν_d	$\nu\sqrt{1-\zeta^2} = 0.0024237$	rad/s
M	1	kg
$\mathbf{J}$	$\mathrm{diag}([0.9516, 0.9203, 0.0527])$	$\mathrm{kg}\cdot\mathrm{m}^2$
k_s	0.1	1/s
$\mathbf{K}_\omega$	$\mathbf{I}_3$	N·m·s
C_D	2.2	–
$\mathbf{H}$	$\mathbf{I}_3$	–
p	$1 \cdot 10^6$	–
γ	0.5	–
$\boldsymbol{\epsilon}$	$[1, 1, 1]^\top \cdot 10^{-3}$	–
ζ	0.0257	–

TABLE IV
INITIAL CONDITIONS

Qty.	Value	Units
$\boldsymbol{r}^i$	$[6718.5, 7.2539 \cdot 10^{-14}, 1184.6]^\top$	km
$\boldsymbol{v}^i$	$[-1.3203, 4.6355 \cdot 10^{-16}, 7.5704]^\top$	km/s
$\boldsymbol{\omega}$	$[0, 0, 0]^\top$	rad/s
S	727.62	cm^2
$\hat{\boldsymbol{m}}$	$[1, 1, 1]^\top$	–
$\boldsymbol{q}$	$[0.3553, 0.4635, 0.8061, 0.0959]^\top$	–
$\mathbf{R}$	$(q_4^2 - \|\boldsymbol{q}_{1:3}\|^2)\mathbf{I}_3 + 2\boldsymbol{q}_{1:3}\boldsymbol{q}_{1:3}^\top - 2q_4\boldsymbol{\mathcal{S}}(\boldsymbol{q}_{1:3})$	–
$\boldsymbol{\eta}$	$[0.56999, 0.8068, 0.1559]^\top$	–

VIII. CONCLUSIONS

In this work, we addressed the regulation of a spacecraft's ES through attitude maneuvers to enable drag-based orbital control. A compact ES definition and its associated dynamics were introduced, forming the basis for an integrator backstepping controller that guarantees the stability of the closed-loop equilibrium points of the ES and rotational dynamics.

Configuration belonging is enforced through control barrier functions embedded in a quadratic programming framework, which preserves the feasibility of the control input while maintaining the stability properties of the nominal controller.

Simulation results confirm the effectiveness of the proposed approach, which provides a unified framework for stable and constraint-aware ES tracking.

ACKNOWLEDGMENT

This work was funded by the Research Council of Norway through the project 335832 QBDebris: A CubeSat formation for space debris characterization [29].

REFERENCES

[1] M. Horsley, S. Nikolaev, and A. Pertica, "Small Satellite Rendezvous Using Differential Lift and Drag," *Journal of Guidance, Control, and Dynamics*, vol. 36, no. 2, pp. 445–453, 2013.
[2] D. Ivanov, M. Kushniruk, and M. Ovchinnikov, "Study of satellite formation flying control using differential lift and drag," *Acta Astronautica*, vol. 152, pp. 88–100, 2018.
[3] T. D. Maclay and C. Tuttle, "Satellite stationkeeping of the ORBCOMM constellation via active control of atmospheric drag: operations, constraints, and performance," *Advances in the Astronautical Sciences*, vol. 120, no. 1, pp. 763–773, 2005.
[4] C. Foster, H. Hallam, and J. Mason, "Orbit determination and differential-drag control of Planet Labs CubeSat constellations," in *AIAA Astrodynamics Specialist Conference, Vail, Colorado, USA, 9-13 August 2015*.
[5] B. Smith, R. Boyce, and M. Brown, "Fast Aerodynamic Establishment of a Constellation of CubeSats," in *7th European Conference for Aeronautics and Space Sciences*, Milan, Italy, 3-6 July 2017.
[6] A. Harris and H. Schaub, "Differential lift and drag constellation control using trimmed attitude," in *29th AAS/AIAA Spaceflight Mechanics Meeting, Maui, Hawaii, USA, 13-17 January 2019*.
[7] D. N. J. Du-Toit, J. J. Du Plessis, and W. H. Steyn, "Using atmospheric drag for constellation control of Low Earth Orbit micro-satellites," in *Small Satellite Conference*, Logan, Utah, USA, 17-19 September 1996.
[8] R. Sun, J. Wang, D. Zhang, Q. Jia, and X. Shao, "Roto-Translational Spacecraft Formation Control Using Aerodynamic Forces," *Journal of Guidance, Control, and Dynamics*, vol. 40, no. 10, pp. 2556–2568, 2017.
[9] C. Riano-Rios, A. Fedele, and R. Bevilacqua, "Roto-translational control of spacecraft in Low Earth Orbit using environmental forces and torques," *Applied Sciences*, vol. 11, no. 10, pp. 4606–4627, 2021.
[10] J. Wang and Z. Sun, "6-DOF robust adaptive terminal sliding mode control for spacecraft formation flying," *Acta Astronautica*, vol. 73, pp. 76–87, 2012.
[11] R. Kristiansen, P. J. Nicklasson, and J. T. Gravdahl, "Formation modelling and 6DOF spacecraft coordination control," in *2007 American Control Conference*, New York City, USA, 11-13 July 2007.
[12] R. Kristiansen, E. I. Grøtli, P. J. Nicklasson, and J. T. Gravdahl, "A model of relative translation and rotation in leader-follower spacecraft formations," *Modeling, Identification and Control*, vol. 28, no. 1, pp. 3–14, 2007.
[13] C. L. Leonard, W. M. Hollister, and E. V. Bergmann, "Orbital Formationkeeping with Differential Drag," *Journal of Guidance, Control, and Dynamics*, vol. 12, no. 1, pp. 108–113, 1989.
[14] B. S. Kumar, A. Ng, K. Yoshihara, and A. De Ruiter, "Differential Drag as a Means of Spacecraft Formation Control," *IEEE Transactions on Aerospace and Electronic Systems*, vol. 47, no. 2, pp. 1125–1135, 2011.
[15] M. S. Shouman and A. M. Atallah, "Control of high fidelity linearized model for satellite formation flight using aerodynamic drag," in *AAS/AIAA Astrodynamics Specialist Conference, Long Beach, California, USA, 13-16 September 2016*.
[16] A. Harris, E. Burnett, and H. Schaub, "Desensitized Optimal Attitude Guidance for Differential-Drag Rendezvous," in *AAS/AIAA Astrodynamics Specialist Conference*, Portland, Maine, USA, 11-15 August 2019.
[17] A. T. Harris, C. D. Petersen, and H. Schaub, "Linear coupled attitude-orbit control through aerodynamic drag," *Journal of Guidance, Control, and Dynamics*, vol. 43, no. 1, pp. 122–131, 2020.
[18] H. D. Curtis, *Orbital Mechanics for Engineering Students*, 2020.
[19] F. L. Markley and J. L. Crassidis, *Fundamentals of Spacecraft Attitude Determination and Control*. Springer New York, 2014.
[20] E. Canuto, C. Novara, D. Carlucci, C. P. Montenegro, and L. Massotti, *Spacecraft Dynamics and Control*, 2018.
[21] O. Ben-Yaacov, E. Edlerman, and P. Gurfil, "Analytical technique for satellite projected cross-sectional area calculation," *Advances in Space Research*, vol. 56, no. 2, pp. 205–217, 2015.

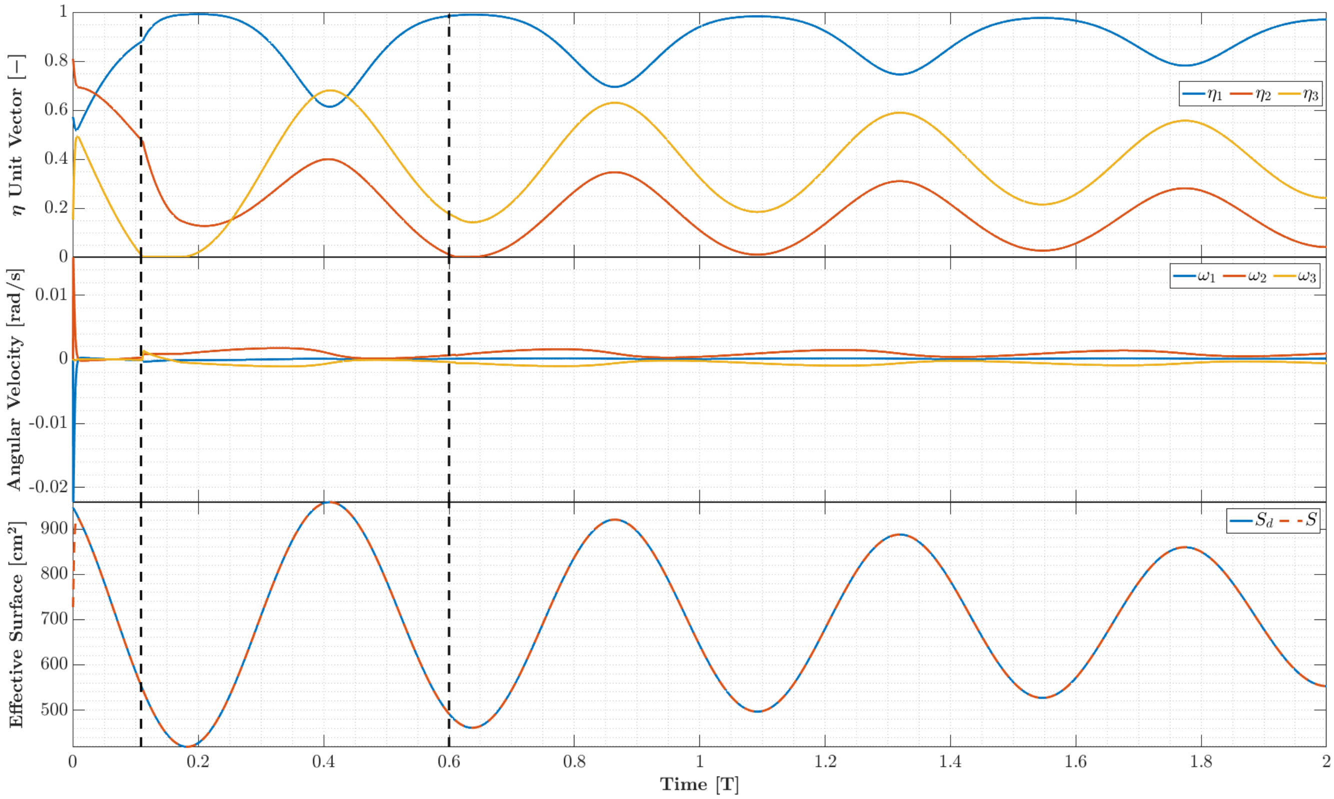

Fig. 2. $\boldsymbol{\eta}$ and $\boldsymbol{\omega}$ components, and ES surface.

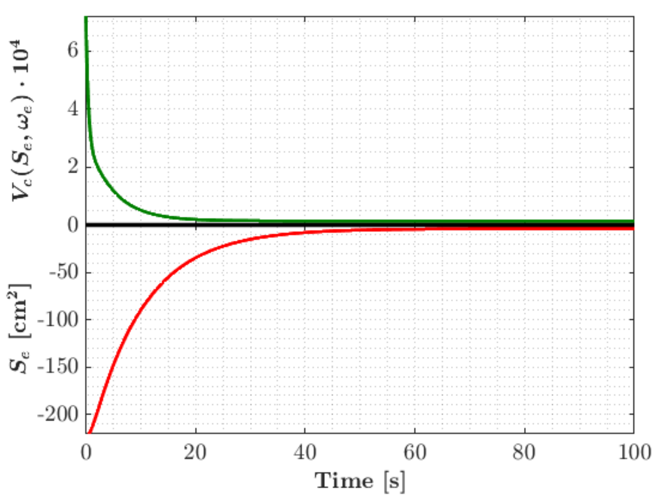

Fig. 3. Composite Lyapunov function and ES error.

[22] R. Schlanbusch, E. I. Grøtli, A. Loria, and P. J. Nicklasson, "Hybrid attitude tracking of rigid bodies without angular velocity measurement," *Systems & Control Letters*, vol. 61, no. 4, pp. 595–601, 2012.

[23] R. Schlanbusch and E. I. Grøtli, "Hybrid certainty equivalence control of rigid bodies with quaternion measurements," *IEEE Transactions on Automatic Control*, vol. 60, no. 9, pp. 2512–2517, 2014.

[24] H. K. Khalil, *Nonlinear Systems*. Prentice Hall, 2002.

[25] I. R. Shafarevich and A. O. Remizov, *Linear algebra and geometry*. Springer Science & Business Media, 2012, ch. 2, p. 56.

[26] A. D. Ames, S. Coogan, M. Egerstedt, G. Notomista, K. Sreenath, and P. Tabuada, "Control barrier functions: Theory and applications," in *18th European Control Conference (ECC)*, 2019, pp. 3420–3431.

[27] W. Xiao, C. G. Cassandras, and C. Belta, *Safe autonomy with control barrier functions: theory and applications*. Springer, 2023.

[28] D. Vallado, *Fundamentals of Astrodynamics and Applications*. Microcosm Press, 2022.

[29] UiT - The Arctic University of Norway , "A CubeSat formation for space debris characterisation (QBDebris)," 2023. [Online]. Available: https://uit.no/project/qbdebris